01 Aug 2022

A SPICE-Compatible Model to Simulate RFI-Induced Buzz Noise Problem in a Camera

Wei Zhang

Shengxuan Xia

Xin Fang

Xu Wang

et. al. For a complete list of authors, see https://scholarsmine.mst.edu/ele_comeng_facwork/4633

Recommended Citation

W. Zhang et al., "A SPICE-Compatible Model to Simulate RFI-Induced Buzz Noise Problem in a Camera," *IEEE Transactions on Electromagnetic Compatibility*, vol. 64, no. 4, pp. 987 - 998, Institute of Electrical and Electronics Engineers, Aug 2022.

The definitive version is available at https://doi.org/10.1109/TEMC.2022.3160926

A SPICE-Compatible Model to Simulate RFI-Induced Buzz Noise Problem in a Camera

Wei Zhang, *Student Member, IEEE*, Shengxuan Xia, *Graduate Student Member, IEEE*, Xin Fang, *Graduate Student Member, IEEE*, Xu Wang, *Graduate Student Member, IEEE*, Takashi Enomoto, Hideki Shumiya, Kenji Araki, *Senior Member, IEEE*, and Chulsoon Hwang, *Senior Member, IEEE*

***Abstract*—This article proposed a SPICE-compatible model to fast simulate the buzz noise problem in a camera device. Based on the reciprocity theorem, the proposed SPICE-compatible model consists of cascaded scattering (S) parameters extracted from the field coupling. It can provide an accurate estimation of the buzz noise transfer function (TF_{total}) between the radio-frequency antenna and the audio system within an average error of 1 dB. Besides, the proposed model allows for coupling decomposition by separating the audio system into different regions, fast buzz noise mitigation by adding filtering circuits, and fast antenna evaluation/selection by characterizing the TF_{total} with different antenna structures. The advantage of the proposed model is that, instead of multiple 3-D simulations during the predesign-stage troubleshooting, it is a fast SPICE-compatible method with SPICE simulation time of 4.5 min and one-time 3-D full-wave simulation on the camera system studied. It provides quick estimation on the potential buzz noise problems, coupling decomposition, buzz noise mitigation methods, and selection of antenna structures.**

***Index Terms*—Buzz noise, radio-frequency interference (RFI), reciprocity theorem, SPICE-compatible model, transfer function.**

I. Introduction

BUZZ is a common issue in wireless devices, such as tablets, laptops, hearing aids, and cameras. It is a periodic noise that can be heard in the audio signal when wireless communication is operating in the system, such as global system for mobile communication (GSM) or WiFi. In 1996 and 1998, the buzz noise was studied in hearing aids exposed under the fields of a transmitting (GSMs) phone at different distances [1], [2]. In [3] and [4], primary mechanisms for causing the audio buzz noise were discussed to be the time-division multiple access (TDMA) signal from the mobile phone, which was a 217-Hz repetition rate pulse signal modulated to the 800–900 MHz and 1800–1900 MHz RF bands. The 217-Hz signal could affect the audio system through the power/ground ripple and radio-frequency (RF) coupling [3], [4]. Studies in [5]–[7] proposed a square-law demodulation mechanism that generates the buzz noise in the wireless systems due to the nonlinear components, such as the input transistors of an amplifier in the audio system. Based on the measurement results of a peacemaker interacting with the modulated and nonmodulated RF signal, Barbaro *et al.* [8] observed that the generation of buzz noise occurred only with a modulated RF signal. It proposed a hypothesis that the demodulation could take place at the overvoltage protection diodes at the input stage of a sensing amplifier. In [9] and [10], the ground distribution network model was proposed to estimate and analyze the audible ground noise caused by TDMA RF power amplifier in an audio circuit.

The characterization of the RF coupling between the aggressor (antenna) and victim (audio system) is necessary to understand the coupling mechanism and investigate the methods to mitigate buzz noise. Reciprocity theorem is a common way to estimate RF interference (RFI) by using the electric (E) and magnetic (H) fields on the defined Huygens box in the forward and reverse problem when exciting the aggressor and the victim, respectively [12]–[18].

To mitigate the buzz noise generated by the RF coupling from the GSM/WiFi antenna to the audio system, two directions can be considered, which are as follows.

1) By changing the physical structure of aggressor or victim to reduce the RF coupling. By rotating the noise source to a certain angle, a minimal RF coupling between the aggressor and the victim was achieved [18], [19].
2) By adding filtering circuits in the audio system [3], [4] [20]–[23].

In the practice, troubleshooting and mitigating the RFI-induced buzz noise at the late stage of a product incurs additional effort and cost. Moreover, to the authors' knowledge, currently the evaluation on potential buzz noise in the early design stage of a product relies mainly on three-dimension (3-D) simulation, which is also time-consuming. Therefore, a fast and effective method is needed for predicting and mitigating the RFI-induced buzz noise during the early design stage.

The novelty of the study in this article is that a circuit model based on reciprocity theorem is proposed to achieve rapid simulation on buzz noise problem of a camera product during the predesign stage in terms of the following:

Manuscript received 1 October 2021; revised 30 January 2022; accepted 27 February 2022. Date of publication 6 May 2022; date of current version 15 August 2022. This work was supported by the National Science Foundation under Grant IIP-1916535. *(Corresponding author: Chulsoon Hwang.)*

Wei Zhang, Shengxuan Xia, Xin Fang, Xu Wang, and Chulsoon Hwang are with the EMC Laboratory, Missouri University of Science and Technology, Rolla, MO 65409 USA (e-mail: wznkm@umsystem.edu; sx7c3@umsystem.edu; fangxin@umsystem.edu; xw7dh@umsystem.edu; hwangc@mst.edu).

Takashi Enomoto, Hideki Shumiya, and Kenji Araki are with the Sony Global Manufacturing & Operations Corporation, Tokyo 108-0075, Japan (e-mail: takashi.enomoto@sony.com; hideki.shumiya@sony.com; kenji.araki@sony.com).

Color versions of one or more figures in this article are available at https://doi.org/10.1109/TEMC.2022.3160926.

Digital Object Identifier 10.1109/TEMC.2022.3160926

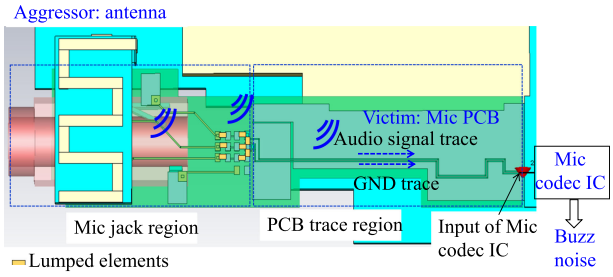

Fig. 1. 3-D model of the camera under investigation.

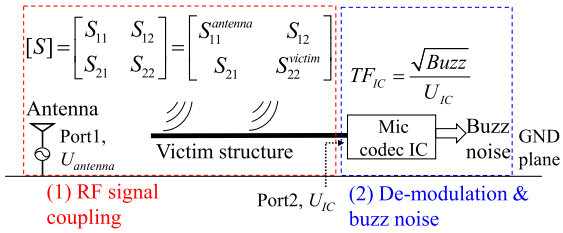

Fig. 2. Diagram of the problem.

1) estimation on the RFI-induced buzz noise or transfer function between the buzz noise and RF signal;
2) analysis on the coupling contribution from the antenna to different regions of the victim;
3) mitigation on the induced buzz noise; and
4) estimation on the induced buzz noise with different antenna structures for antenna selection.

The model can be simulated in any circuit/SPICE simulators allowing for importing the S-parameter files as a symbol or block and embedding them in simulation.

The rest of this article is organized as follows: Section II describes the problem and the overall procedure. Section III introduces the proposed circuit model to estimate the transfer function for the WiFi-induced buzz noise. In Section IV, applications for the proposed model are shown and discussed, including the mitigation of buzz noise and the feasibility of fast predicting the buzz noise transfer function when the antenna structure (aggressor) is changed. Finally, Section V concludes this article.

II. Problem Description and Definition

Fig. 1 shows a 3-D model of the camera system under investigation. It contains a meander-shaped WiFi antenna placed on top of the audio PCB, which includes an external microphone (Mic) jack (audio jack region), traces of the audio signal path (PCB trace region), and a Mic codec IC that converts the analog audio signal to digital signal. In this system, it was observed by the authors that the modulated WiFi signal could couple to the audio signal paths due to the compact geometry. The nonlinear behavior of the Mic codec IC demodulated the coupled WiFi noise into a low-frequency baseband signal via a square function [5]–[7]. The low-frequency components within the audible range ($<$ 20 kHz) in the demodulated signal acts as buzz noise in the audio signal. As the mechanism of buzz noise generation between the WiFi antenna and the audio paths of two channels (left, right) are similar, here we are focusing on investigating the induced buzz noise in one channel.

The entire study is based on the following assumptions, which helps simplify the problem while maintaining the main characteristics of the camera under normal operation conditions.

1) The bias voltage and source/load impedances are assumed to be fixed. No nonlinearity from these variations is ignored. This is because every product (same model) has the same configuration (source/load impedances and bias voltage). Although the modeling approach in this article can be extended to different products, the authors do not expect to apply the same buzz noise behavior (characterized on one type of IC) to products with different Mic codec ICs.
2) It is assumed that the WiFi-coupled noise signal that inputs to the Mic codec IC is small enough such that the nonlinear behavior can be sufficiently modeled as a square function. This is the case in the mobile cellphones where the Tx power do not exceed 23 dBm. This was tested and validated in [6]. In this article, the excitation power of the WiFi antenna under normal operation is 7–17 dBm, which is expected to satisfy this assumption.
3) It is assumed that the buzz noise response of the Mic codec IC is not changing with the baseband frequency (50 Hz–11 kHz) of the input modulated signal, this is proved by measuring the buzz noise transfer function when injecting the modulated signal to Mic codec IC with 2.4-GHz carrier frequency and swept baseband frequency. The result is shown in Fig. 21, Appendix A.

As shown in Fig. 2, the problem was decomposed in two parts: First, coupling of RF noise from WiFi antenna to the audio system; second, demodulation of the coupled RF noise. The total transfer function ($\mathrm{TF_{total}}$, unit: 1/V) between the induced buzz noise in one audio channel and the RF voltage at the antenna port is defined as

$$\mathrm{TF_{total}} = \frac{\sqrt{\mathrm{Buzz}}}{U_{\mathrm{antenna}}} \tag{1}$$

where Buzz is the amplitude (unitless) of the audio signal at two times of the base-band frequency (f_{IF}) when the WiFi antenna is excited by the modulated RF signal (base-band frequency: f_{IF}; local-oscillator frequency: f_{LO}) [6], [7]; U_{antenna} (unit: V) is the total excitation voltage at the modulated frequency ($f_{\mathrm{LO}} \pm f_{IF}$) looking at the input port of the WiFi antenna.

Since the buzz noise is generated by the demodulation effect of the Mic codec IC, which is equivalent to an operation of square function on the coupled RF noise voltage [6], [7], instead of the amplitude of buzz noise (Buzz), the square root of buzz noise ($\sqrt{\mathrm{Buzz}}$) is used to calculate $\mathrm{TF_{total}}$ with U_{antenna}.

The coupling of RF noise between the antenna and audio system can be expressed by the scattering (S) parameter matrix between the antenna input port (Port 1) and the audio input port (Port 2) of the Mic codec IC in one channel. Based on the signal

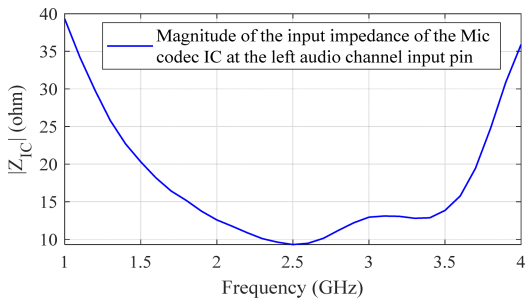

Fig. 3. Magnitude of input impedance of the audio input (left channel) in Mic codec IC ($|Z_{IC}|$).

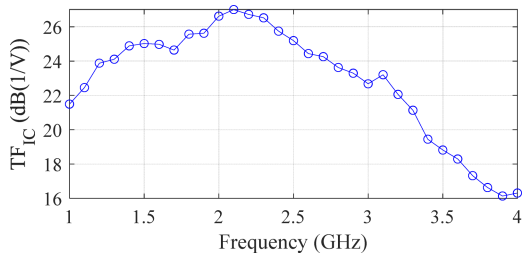

Fig. 4. Buzz noise transfer function of the Mic codec IC (TF_{IC}).

flow graph, $\mathrm{TF}_{\mathrm{total}}$ can be further expressed as

$$\mathrm{TF}_{\mathrm{total}} = \frac{\sqrt{\mathrm{Buzz}}}{U_{\mathrm{antenna}}} = \frac{\sqrt{\mathrm{Buzz}}}{U_{IC}} \cdot \left| S_{21} \cdot \frac{(1+\Gamma)}{(1+S_{11})(1-S_{22}\Gamma)} \right| = \mathrm{TF}_{IC} \cdot |S_{21}| \cdot \left| \frac{(1+\Gamma)}{(1+S_{11})(1-S_{22}\Gamma)} \right| \quad (2)$$

where U_{IC} (unit: V) is the total voltage at the audio input (left channel) of Mic codec IC at the modulated frequency. S_{21} represents the coupling between the aggressor port (input of the WiFi antenna, Port 1) and the victim port (the left-channel audio input of Mic codec IC, Port 2). S_{11} and S_{22} represents the reflection coefficient at Port 1 and Port 2. Γ is the reflection coefficient when Port 2 is terminated with the input impedance (Z_{IC}, unit: Ω) of the Mic codec IC, as is shown in the following:

$$\Gamma = \frac{Z_{IC} - Z_0}{Z_{IC} + Z_0} \quad (3)$$

where $Z_0 = 50\ \Omega$.

The measured input impedance (Z_{IC}) of the Mic codec IC for the audio input in the left channel is shown in Fig. 3.

TF_{IC} (unit: 1/V) is the transfer function between the generated buzz noise and the RF noise voltage at the audio input of the Mic codec IC, which characterizes the demodulation/nonlinearity effect of the Mic codec IC. It is defined in the following:

$$\mathrm{TF}_{IC} = \frac{\sqrt{\mathrm{Buzz}}}{U_{IC}}. \quad (4)$$

The TF_{IC} can be extracted from measurement. As discussed in [6, Fig. 4], using a mixer and band pass filter, a three-tone RF signal with modulation was created. When the audio path at the Mic PCB is disconnected with the Mic codec IC, the modulated RF signal ($f_{IF} = 1$ kHz, $f_{\mathrm{LO}} = 1$–4 GHz) was directly injected at the input port of the Mic codec IC. The buzz noise was extracted from the amplitude of the 2-kHz component in the spectrum of the recorded audio signal. The measured TF_{IC} is shown in Fig. 4. Detailed measurement procedure of TF_{IC} is shown in Appendix A.

From (1), since TF_{IC} and Z_{IC} is fixed and can be measured directly with the Mic code IC, the RF coupling between the WiFi antenna and the audio path in the Mic PCB is the only undetermined factor that affects the induced buzz noise, which can be expressed in a circuit representation and is introduced in Section III. Therefore, a SPICE-compatible model, including the coupling between RF antenna and audio system, TF_{IC}, and Z_{IC} can be established to quickly predict the total buzz noise transfer function or the induced buzz noise with a certain RF excitation voltage at the antenna side.

III. Circuit Representation of WiFi-Caused Buzz Noise

The coupling between the WiFi antenna and audio path (victim structure) in the Mic PCB can be decomposed into two regions: Mic jack region and PCB (audio) trace region. The total coupling ($S_{21\mathrm{total}}$) between the WiFi antenna and audio path can be modeled by cascading the S-parameters representing the coupling between the WiFi antenna and the different regions of the audio path. In this way, the $S_{21\mathrm{total}}$ and the coupling contribution between the WiFi antenna and the different regions of the audio path can be evaluated.

A. Step 1: Cascaded S-Parameters From Physical Geometry

In the first step, a proof of concept was performed from the physical geometry of the Mic PCB using a SPICE model with cascaded S-parameters. As is shown in Fig. 5(a), for ports were created for simulation in the 3-D model of the camera. Specifically, in Fig. 5(b), the antenna excitation port was defined as Port 1, which was located between the spring contact (simplified as a metal cuboid in the 3-D model) of the antenna and the ground plane of the main board. In addition, in Fig. 5(b), the victim port (Port 2) was defined between the end of the audio signal trace (e.g., the left channel audio path) and the ground trace in the audio circuit, which was also connected to the audio and ground input of the Mic codec IC. Moreover, as is shown in Fig. 5(c), the lumped element "LP1" was removed in the simulation model and the audio path was cut into two regions: the Mic jack region and the audio trace region. Therefore, two internal ports were created as Port 3 and Port 4 in Fig. 5(c). The Port 3 was defined between the end of audio path in the Mic jack region and the ground. The Port 4 was defined between the start position of the audio path in the PCB (audio) trace region and the ground. Therefore, a four-port S-parameter simulation could be performed in CST Microwave Studio [24] and a cascaded S-parameter model was created in Agilent Advanced Design System 2017 (ADS 2017) [25] to simulate the total coupling and the individual coupling from WiFi antenna to different regions of the victim.

The circuit model is shown in Fig. 6. As the 3-D simulation in CST generates four-port S-parameter matrix, the circuit model used two identical four-port S-parameter matrices $[\mathrm{S}]_1$ and $[\mathrm{S}]_2$

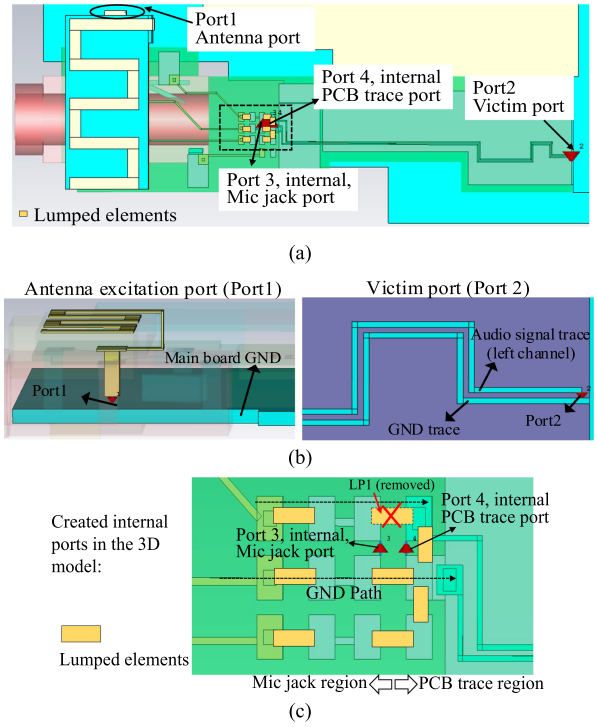

Fig. 5. 3-D model of the four-port simulation. (a) Overview of the defined ports. (b) Definition of ports at antenna side and victim side. (c) Definition of internal ports at the adjunct region of Mic jack and PCB trace.

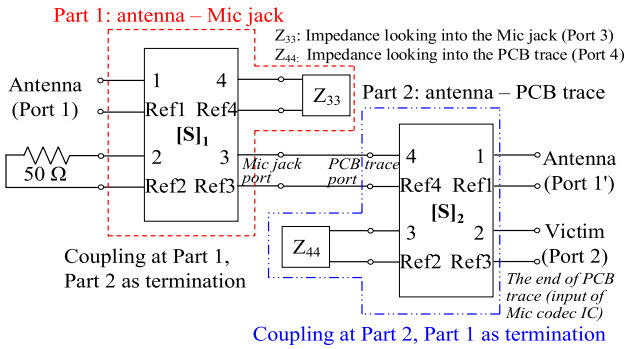

Fig. 6. Circuit model of the cascaded S-parameters from physical geometry.

representing the coupling from antenna to the Mic jack region (Part 1) and the PCB trace region (Part 2). Port 3 of $[S]_1$ represents the end of the audio path in the Mic jack region, which intends for "*Mic jack port*" in Fig. 6. Port 4 of $[S]_2$ is defined at the start location of the audio trace in the PCB trace region, which intends for "*PCB trace port*" in Fig. 6. Port 2 of $[S]_2$ is named as "Victim port," which represents the end location of the audio path in PCB trace region that connects to the input of the Mic codes IC.

$[S]_1$ and $[S]_2$ were cascaded through the internal ports (i.e., Port 3 of $[S]_1$ was connected to the Port 4 of $[S]_2$) to complete the audio path from Mic jack region to PCB trace region. The unused port, such as Port 4 of $[S]_1$, was terminated with the impedance looking into the Mic jack region (Z_{33} at the Port 3 in

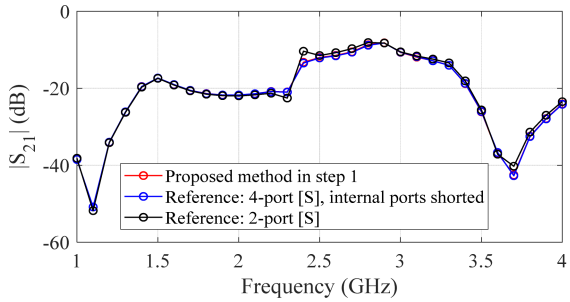

Fig. 7. $|S_{21\text{total}}|$ comparison between the proposed cascaded S-parameter model, two-port direct simulation, and four-port simulation with the internal ports shorted.

Fig. 5) to maintain the same condition as the actual scenario. Port 2 of $[S]_1$ was also unused, which was terminated with 50 Ω. Similarly, the Port 3 of $[S]_2$ was terminated with the impedance looking into the PCB trace region (Z_{44} at the Port 4 in Fig. 5). Individual antenna ports (Port 1 and Port 1') were applied to the two S-parameter matrices to simulate the coupled voltage at the victim port (i.e., the end of the audio path in PCB trace region that connected to the input of the Mic codec IC), which was contributed by the coupling from antenna to Mic jack region and from antenna to the PCB trace region, respectively. The impedance at the internal nodes was handled by the cascading operation. Therefore, when exciting the antenna port (Port 1) in $[S]_1$ and keep the antenna port (Port 1') of $[S]_2$ unexcited/terminated with 50 Ω, the voltage obtained at the end of the audio path in the Mic jack region (Port 3 of $[S]_1$) can be transferred to the victim port (Port 2 of $[S]_2$) via $[S]_2$, which represents the coupling from the antenna to the Mic jack region. Similarly, when exciting the antenna port (Port 1') in $[S]_2$ and keep the antenna port (Port 1) of $[S]_1$ unexcited/terminated with 50 Ω, the coupled voltage at the victim port (Port 2 of $[S]_2$) can be obtained as the coupling from the antenna to the PCB trace region. The RF coupled voltages at the victim port (Port 2) were simulated by exciting each antenna port in $[S]_1$ (Port 1 in Fig. 6) and $[S]_2$ (Port 1 in Fig. 6), which are the coupling from the antenna—Mic jack region and antenna—PCB trace region, respectively. The total coupling ($S_{21\text{total}}$) between the antenna and the victim can be expressed as

$$S_{21\text{total}} = S_{21} + S_{21'}. \tag{5}$$

Fig. 7 shows the total coupling between the antenna and the victim ($|S_{21\text{total}}|$) from the proposed cascaded S-parameters in step 1, the 2-port S-parameter matrix from direct simulation between antenna port and victim port in CST, and the four-port S-parameter matrix with the internal ports shorted. The proposed model in step 1 shows an accuracy of 0 dB compared to $|S_{21\text{total}}|$ simulated from four-port S-parameter, and an accuracy of 0.6 dB average error compared to $|S_{21\text{total}}|$ simulated from the four-port direct simulation in CST. The discrepancy is caused by the operation of cutting the audio path to create the internal nodes in the 3-D model.

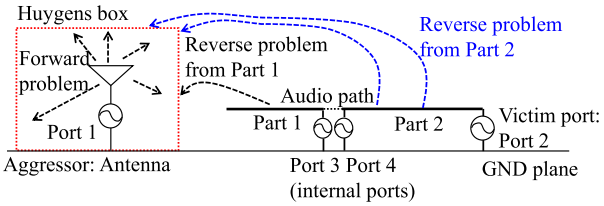

Fig. 8. Diagram of the problem based on the reciprocity theory.

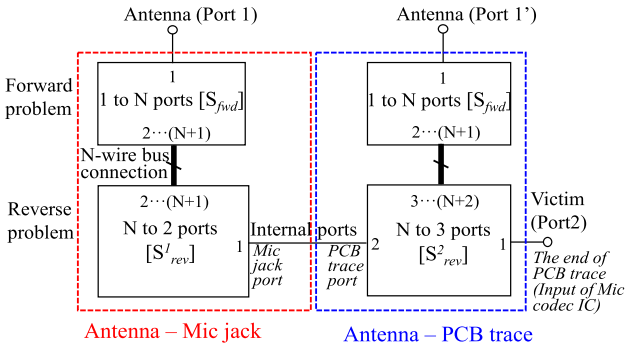

Fig. 9. Circuit model of the cascaded S-parameters based on field coupling.

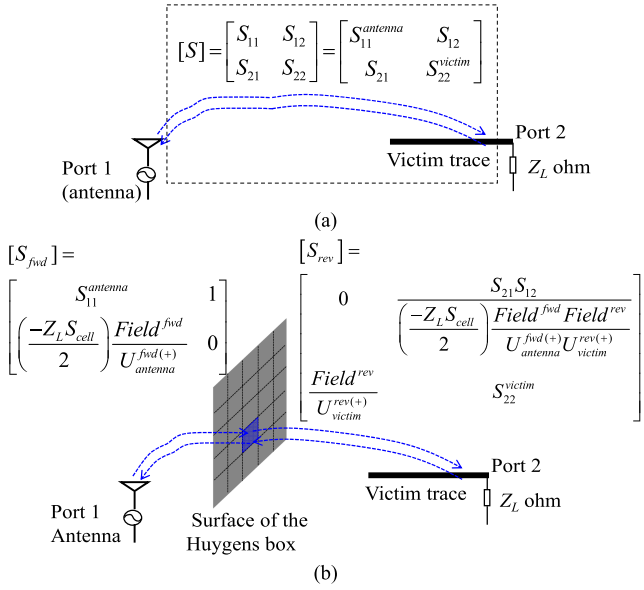

Fig. 10. (a) Original problem. (b) Separated problem: cascaded [S] based on the field terms in reciprocity theory.

B. Step 2: Cascaded S-Parameters From Field Coupling

Furthermore, the proposed method of cascaded S-parameters was extended to the RF field coupling representation based on the reciprocity theorem. As shown in Fig. 8, the noise coupling between the antenna and different regions of the audio path in the Mic PCB was expressed by the fields on the surfaces of the Huygens box in the forward and reverse problem, where the antenna port (Port 1 in Fig. 8) was excited in the forward problem and the victim port (Port 3 or Port 2 in Fig. 8) was excited in the reverse problem.

According to the reciprocity theorem, the fields ($\mathbf{H}_c^{fwd}$, $\mathbf{E}_c^{fwd}$, $\mathbf{H}_c^{rev}$, and $\mathbf{E}_c^{rev}$) on each discretized cell (cell area of S_{cell}) of the surfaces of Huygens box in the forward and reverse problem were used to calculate the total coupling [11]–[13]

$$S_{21\text{total}} = \frac{U_{\text{victim}}^{\text{fwd}(+)}}{U_{\text{antenna}}^{\text{fwd}(+)}} = \frac{-Z_L}{2}\frac{1}{U_{\text{antenna}}^{\text{fwd}(+)}U_{\text{victim}}^{\text{rev}(+)}}\sum_{\text{cells}}\begin{pmatrix}\hat{n}\times\mathbf{H}_c^{\text{fwd}}\cdot\mathbf{E}_c^{\text{rev}}+\\ \hat{n}\times\mathbf{E}_c^{\text{fwd}}\cdot\mathbf{H}_c^{\text{rev}}\end{pmatrix}\cdot S_{\text{cell}}. \tag{6}$$

In (6), $U_{\text{antenna}}^{\text{fwd}(+)}$ is the incident voltage at the antenna port in the forward problem; $U_{\text{victim}}^{\text{fwd}(+)}$ is the induced voltage at the victim port in the forward problem; $U_{\text{victim}}^{\text{rev}(+)}$ is the incident voltage at the victim port in the reverse problem; Z_L is the load impedance at the victim port in the receiving mode in the forward problem (50 Ω in $S_{21\text{total}}$ calculation; Z_{IC} in the buzz noise calculation).

From (6), $S_{21\text{total}}$ can be expressed as a circuit model with cascaded S-parameter matrices based on the fields on the discretized cells of the surfaces on the Huygens box and the incident voltages in the forward and reverse problem, as shown in Fig. 9.

The internal ports (Mic jack port and PCB trace port) were cascaded to transfer the coupled noise of antenna—Mic jack region to the victim port (input of the Mic codec IC) through the PCB trace region. Meanwhile, the impedance matching between the internal ports in $[S_{\text{rev}}^1]$ and $[S_{\text{rev}}^2]$ was handled through cascading. Taking each discretized cell of the Huygens box surfaces as a port, the cascaded S-parameter matrices $[S_{\text{fwd}}]$ and $[S_{\text{rev}}]$ were created using the corresponded E and H fields. Individual S-parameter matrices $[S_{\text{rev}}^1]$ and $[S_{\text{rev}}^2]$ can be created in the reverse problem when exciting the Mic jack region (Port 3) or the PCB trace region (Port 2) in Fig. 8. They were connected to $[S_{\text{fwd}}]$ via the port indicating each discretized cell. The internal ports at the internal nodes to separate the Mic jack region and PCB trace region were also handled in $[S_{\text{rev}}^1]$ and $[S_{\text{rev}}^2]$for cascading and impedance matching similar as the original scenario. Individual excitations were added to the antenna port of each cascaded S-parameter block. Based on (6), the model can estimate the coupling from the antenna to the Mic jack region (Part 1), and to the PCB trace region (Part 2), respectively. The total coupling between the antenna and victim will be the addition of the coupling at Part 1 and Part 2.

Fig. 10 shows the original problem with a total S-parameter matrix ([S]) and the separated problem based on the cascaded S-parameter matrices from the field coupling between the antenna and victim, where the S_{11}^{antenna} is the reflection coefficient at the antenna port in the transmitting mode (forward problem); S_{22}^{victim} is the reflection coefficient at the victim port in the transmitting mode (reverse problem); S_{21} and S_{12} represent the coupling between the antenna and victim ports. Taking the forward and reverse field Field$^{\text{fwd}}$ (denotes the scalar field E_c^{fwd} and H_c^{fwd}), Field$^{\text{rev}}$ (denotes the scaler field E_c^{rev} and H_c^{rev}) on one discretized cell as an example, the expressions for $[S_{\text{fwd}}]$ and $[S_{\text{rev}}]$ is shown in Fig. 10(b).

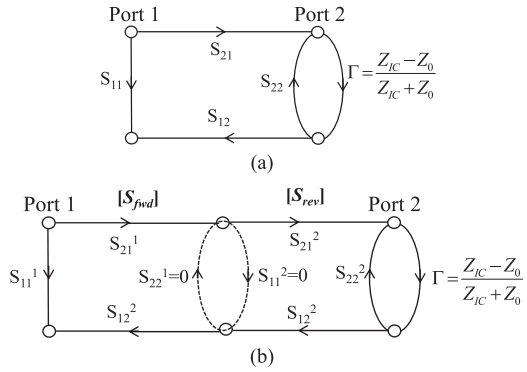

Fig. 11. (a) Signal flow graph of the original problem. (b) Signal flow graph of the cascaded [S] problem based on the field coupling in reciprocity theory.

From the signal flow graph in Fig. 11(a), in the original problem, the total coupling ($S_{21\text{total}}$) and the total reflection coefficient ($S_{11\text{total}}$) at the antenna port in the forward problem is calculated as follows:

$$\begin{cases} S_{11\text{total}} = S_{11} + \frac{S_{21}\Gamma S_{12}}{1-S_{22}\Gamma} \\ S_{21\text{total}} = \frac{S_{21}}{1-S_{22}\Gamma} \end{cases}. \tag{7}$$

In Fig. 11(b), for each discretized cell on the Huygens box surfaces, S_{11} and S_{21} calculated by the cascaded $[S_{\text{fwd}}]$ and $[S_{\text{rev}}]$ from the field coupling based on the reciprocity theorem can be written as

$$\begin{cases} S_{11\text{total}} = \frac{V_1^{1-}}{V_1^{1+}} = S_{11}^1 + \frac{S_{21}^1 S_{21}^2 \Gamma S_{12}^2 S_{12}^1}{1-S_{22}^2\Gamma} \\ S_{21\text{total}} = \frac{V_2^{2-}}{V_1^{1+}} = \frac{S_{21}^1 S_{21}^1}{(1-S_{22}^2\Gamma)} \\ \quad = \left(\frac{-Z_L S_{\text{cell}}}{2} \frac{\text{Field}^{\text{fwd}}}{U_{\text{antenna}}^{\text{fwd}(+)}} \frac{\text{Field}^{\text{rev}}}{U_{\text{victim}}^{\text{rev}(-)}}\right) \frac{1}{1-S_{22}^2\Gamma} \end{cases} \tag{8}$$

where the product of $\text{Field}^{\text{fwd}}$ and $\text{Field}^{\text{rev}}$ is

$$\text{Field}^{\text{fwd}}\,\text{Field}^{\text{rev}} = \sum \left(\hat{n} \times \mathbf{H}_c^{fwd} \cdot \mathbf{E}_c^{rev} + \hat{n} \times \mathbf{E}_c^{fwd} \cdot \mathbf{H}_c^{rev}\right). \tag{9}$$

In addition, as S_{22}^1 and S_{11}^2 are set as 0, S_{11}^1 and S_{22}^2 should be equal toS_{11} and S_{22}in the original problem in Fig. 11(a). Therefore, when considering the superposition of the coupling (S_{21}) through all the cells on the Huygens box surfaces, the proposed method of the cascaded S-parameter matrices from field coupling should provide the same $S_{11\text{total}}$ and $S_{21\text{total}}$ as the initial problem. Assuming the surfaces on the Huygens box are discretized into N cells, mathematically we can write the matrixes $[S_{\text{fwd}}]_{(N+1)\times(N+1)}$ for one port of antenna and N ports for the forward fields on N discretized cells when the antenna is excited. The matrix $[S_{\text{rev}}^1]_{(N+1)\times(N+1)}$includes one port of internal port (Mic jack port) and N ports for the reverse fields on N discretized cells when the Mic jack port is excited. The matrix $[S_{\text{rev}}^2]_{(N+2)\times(N+2)}$includes one port of internal port (PCB trace port), one port of the input of Mic codec IC (Victim port), and N ports for the reverse field on N discretized cells associated when the PCB trace port is excited. The expressions for $[S_{\text{fwd}}]_{(N+1)\times(N+1)}$, $[S_{\text{rev}}^1]_{(N+1)\times(N+1)}$, and $[S_{\text{rev}}^2]_{(N+2)\times(N+2)}$are shown as follows:

$$[S_{\text{fwd}}] = \begin{bmatrix} S_{11} & 1 & \dots & 1 \\ \left(\frac{-Z_L S_{\text{cell}}}{2}\right) \frac{\text{Field}_1^{\text{fwd}}}{U_{\text{antenna}}^{\text{fwd}(+)}} & 0 & 0 & 0 \\ \vdots & \vdots & \vdots & \vdots \\ \left(\frac{-Z_L S_{\text{cell}}}{2}\right) \frac{\text{Field}_N^{\text{fwd}}}{U_{\text{antenna}}^{\text{fwd}(+)}} & 0 & 0 & 0 \end{bmatrix} \tag{10}$$

$$[S_{\text{rev}}^1] = \begin{bmatrix} S_{33} & \frac{\text{Field}_1^{\text{rev}}}{U_{\text{victim}}^{\text{rev}(+)}} & \cdots & \frac{\text{Field}_N^{\text{rev}}}{U_{\text{victim}}^{\text{rev}(+)}} \\ \frac{S_{21}S_{12}}{\frac{-Z_L S_{\text{cell}}}{2} \sum_{i=1:N} \frac{\text{Field}_i^{\text{fwd}}}{U_{\text{antenna}}^{\text{fwd}(+)}} \frac{\text{Field}_i^{\text{rev}}}{U_{\text{victim}}^{\text{rev}(+)}}} & 0 & 0 & 0 \\ 0 & \vdots & \vdots & \vdots \\ \vdots & 0 & 0 & 0 \\ 0 & 0 & 0 & 0 \end{bmatrix} \tag{11}$$

$$[S_{\text{rev}}^2] = \begin{bmatrix} S_{22} & S_{42} & \frac{\text{Field}_1^{\text{rev}}}{U_{\text{victim}}^{\text{rev}(+)}} & \cdots & \frac{\text{Field}_N^{\text{rev}}}{U_{\text{victim}}^{\text{rev}(+)}} \\ S_{24} & S_{44} & 0 & 0 & 0 \\ \frac{S_{21}S_{12}}{\frac{-Z_L S_{\text{cell}}}{2} \sum_{i=1:N} \frac{\text{Field}_i^{\text{fwd}}}{U_{\text{antenna}}^{\text{fwd}(+)}} \frac{\text{Field}_i^{\text{rev}}}{U_{\text{victim}}^{\text{rev}(+)}}} & 0 & 0 & 0 & 0 \\ 0 & \ddots & \vdots & \vdots & \vdots \\ \vdots & \cdots & 0 & 0 & 0 \\ 0 & \cdots & 0 & 0 & 0 \end{bmatrix} \tag{12}$$

where $\text{Field}_i^{\text{fwd}}$ and $\text{Field}_i^{\text{rev}}$ are the forward and reverse field on the ith cell of the Huygens box; "S_{11}" in $[S_{\text{fwd}}]$ intends for the reflection coefficient at the antenna port simulated by the model in Fig. 5. "S_{33}" in $[S_{\text{rev}}^1]$intends for the reflection coefficient at the Mic jack port simulated by the model in Fig. 5; "S_{22}" and "S_{44}" in $[S_{\text{rev}}^2]$intend for the reflection coefficient at the victim port (input of the Mic codec IC) and the PCB trace port, respectively, which are simulated by the model in Fig. 5. Similarly, "S_{24}" and "S_{42}" in $[S_{\text{rev}}^2]$are the transmission coefficient between the victim port and the PCB trace port.

After cascading the $[S_{\text{fwd}}]$ and $[S_{\text{rev}}]$ with the discretized cells of the Huygens box surfaces, the proposed model can automatically generate the total coupling $S_{21\text{total}}$ the same as the equation to calculate the total coupling based on the reciprocity theory in (6). The reflections from the victim to the antenna port is also handled in $[S_{\text{fwd}}]$ and $[S_{\text{rev}}]$.

For the camera studied in this article, a six-surface Huygens box was defined around the antenna region with the size and step listed in Table I. The proposed cascaded model in Fig. 9 can be expressed in a SPICE-compatible way. As shown in Fig. 12, it can predict the total coupling $|S_{21\text{total}}|$ with an average error of 1.1 dB compared to the results of the two-port S-parameter from the CST direct simulation.

Furthermore, this model can decompose the coupling between the antenna and different regions of the Mic PCB structure. Fig. 13 shows the $|S_{21}|$ contributed from the coupling between the antenna and the Mic jack region, and between the antenna and

TABLE I
HUYGENS BOX SIZE AND STEP SIZE

Direction	# of cells along each direction	Huygens box range in each direction (mm)	Step (mm)
X	13	[42.3, 54.7]	1.033
Y	23	[-29.7, -14.3]	0.7
Z	11	[-10.75, -3.75]	0.7

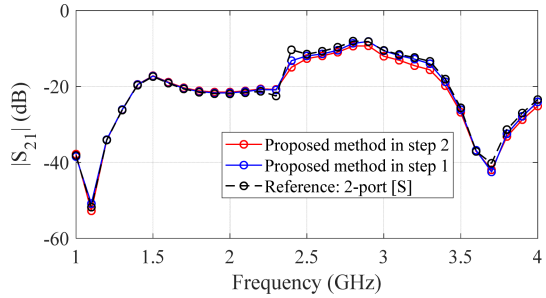

Fig. 12. Comparison of $|S_{21\text{total}}|$ between the proposed model of cascaded S-parameters from field coupling in step 2, step 1, and the two-port S-parameter from CST.

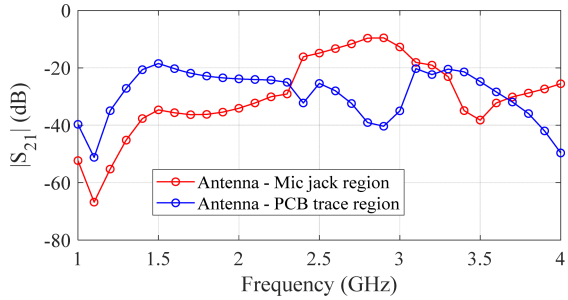

Fig. 13. Coupling between antenna and the Mic jack region, and the antenna and the PCB trace region.

the PCB trace region. It is observed that in the frequency range of 1.0–2.0 GHz, the coupling between the antenna and the PCB trace region dominates the total coupling. In the frequency range of 2.4–3.0 GHz, the total coupling is dominated by the coupling between the antenna and the Mic jack region. Therefore, for the WiFi antenna working around 2.4 GHz, the dominating coupling occurs between the antenna and Mic jack region.

C. Buzz Noise Prediction

Based on (2), the RFI-induced buzz noise can be predicted from the proposed cascaded S-parameter model based on field coupling. Furthermore, the total transfer function can be calculated from (2) given the total voltage at the input port of the antenna.

The circuit model for the buzz noise simulation is shown in Fig. 14 and Appendix B. Individual frequency-domain sources can be added as the antenna excitations in the antenna—Mic jack part and the antenna—PCB trace part. Z_{IC} is connected as the termination at the output of the model (the audio signal input of the Mic codec IC). Therefore, the total voltage at the input

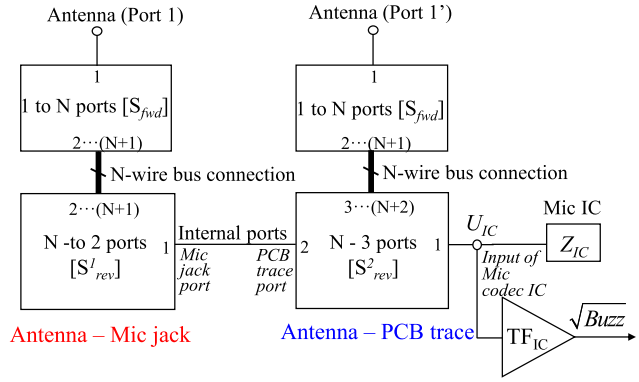

Fig. 14. Proposed circuit model with cascaded S-parameter from field coupling for buzz noise simulation.

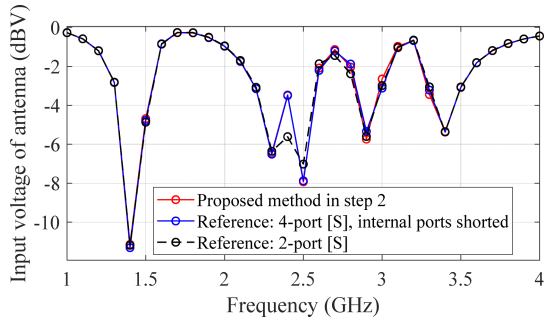

Fig. 15. Comparison of U_{antenna} between the proposed model of cascaded S-parameters from field coupling in step 2, the two-port S-parameter from CST, and the four-port S-parameter from CST with Port 3 and Port 4 shorted.

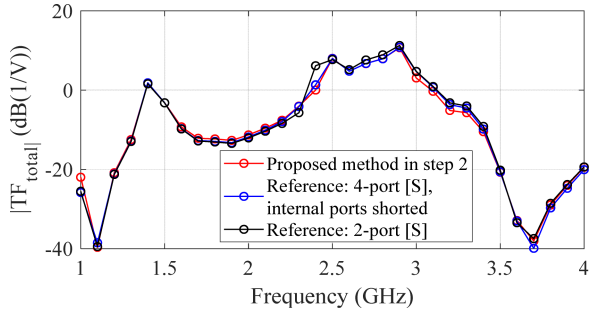

Fig. 16. Comparison of TF_{total} between the proposed model of cascaded S-parameters from field coupling in step 2, the two-port S-parameter from CST, and the four-port S-parameter from CST with Port 3 and Port 4 shorted.

of the Mic codec IC (U_{IC}) can be simulated from the proposed SPICE-compatible model. Using the measured TF_{IC}, the $\sqrt{\text{Buzz}}$ can be known by

$$\sqrt{\text{Buzz}} = U_{IC}\text{TF}_{IC}. \tag{13}$$

Therefore, the TF_{total} can be calculated from (1) with the simulated $\sqrt{\text{Buzz}}$ and U_{antenna}. The simulated U_{antenna} and the calculated TF_{total} are shown in Figs. 15 and 16.

From Figs. 15 and 16, the proposed cascaded S-parameter model from field coupling is in good agreement with the direct

TABLE II
COMPARISON OF THE SIMULATION TIME BETWEEN THE PROPOSED MODEL AND 3-D SIMULATION IN DIFFERENT SCENARIOS

Models		Total simulation time: 1-time simulation	Total simulation time: N-time simulations to mitigate buzz noise via circuit change
3D solver (CST): 2-port model simulation		1.18 h	(N×1.18) h
3D solver (CST): 4-port model simulation		2.5 h	(N×2.5) h
Proposed circuit model in this paper	3D solver (CST): 4-port simulation	2.5 h	No
	Write S-parameter files (MATLAB)	1.6 min	No
	Cascaded S-parameter circuit model simulation (ADS)	4.5 min	4.5 min

wot-port simulation in CST in terms of both the total voltage U_{antenna} at the antenna port (average error of 0.2 dB) and the total transfer function TF_{total} (average error of 1 dB). The descrepancy is caused by the operation of cutting the audio path to create the internal nodes in the 3-D model.

D. Simulation Time

Table II compares the time for buzz noise simulation from the 3-D model in CST, and the proposed SPICE-compatible cascaded S-parameter model from field coupling. Instead of running the time-consuming 3-D simulation for multiple times, the proposed SPICE-compatible model based on field coupling can provide a fast method for predicting, debugging, and mitigating the buzz noise problem in the predesign stage with 4.5-min circuit simulation and only one-time 3-D simulation (2.5 h) to get the fields. Especially for the scenario that buzz noise mitigation is needed on the existing circuit model, such as quick estimations on the buzz noise by adding/changing the lumped circuits in the model for multiple times, the proposed circuit model only takes 4.5 min for each simulation.

IV. APPLICATIONS AND DISCUSSION

The proposed model can allow for fast buzz noise mitigation by adding filtering circuits (decoupling capacitors, inductors, or ferrites) at different locations of the model. Furthermore, it can provide prediction of buzz noise or TF_{total} for fast antenna selection when the antenna structure is changed.

A. Methods of Mitigation on Buzz Noise

Based on the proposed circuit model, the mitigation method for reducing the buzz noise is simulated by adding a decoupling capacitor (100 pF, 0102 package) with parasitic. As shown in Fig. 17, two cases were investigated: adding a shunt decoupling capacitor at the internal node; adding a shunt decoupling capacitor at the input of the Mic codec IC.

The TF_{total} estimated from the two cases is compared with that from the original model without adding the 100-pF capacitor, as shown in Fig. 18. It is observed that when the 100-pF capacitor is added at the internal node, the TF_{total} is reduced significantly in the frequency range of 2.4–3.0 GHz, which provides the buzz noise mitigation in a limited frequency range. This is because the decoupling capacitor at the internal node can only effectively mitigate the coupling between the antenna and the Mic jack region, which dominates the total coupling in 2.4–3.0 GHz. However, when a decoupling capacitor of 100 pF is added at the input of the Mic codec IC, the TF_{total} is reduced in 1–4 GHz. This is because the decoupling capacitor at the end of the coupling path can mitigate all the coupled noise on the whole audio path of the Mic PCB structure.

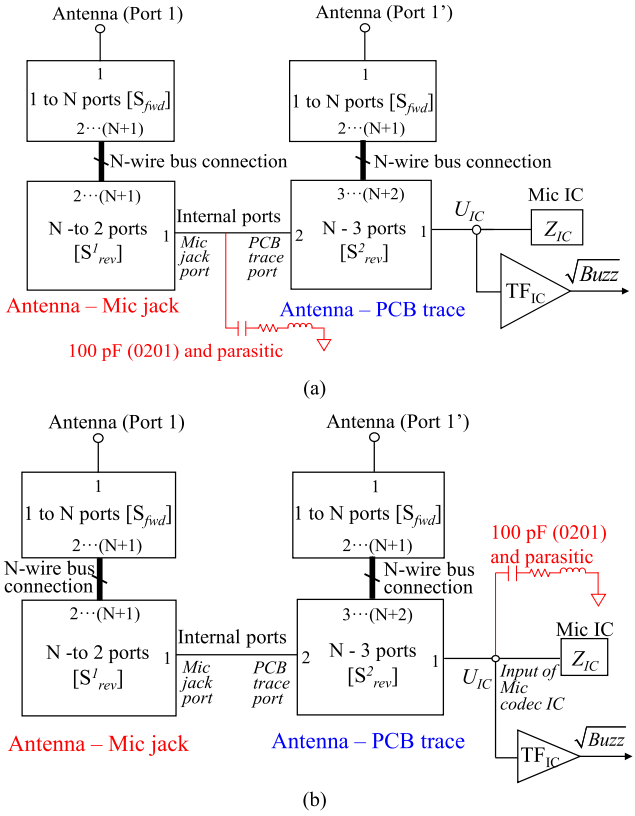

Fig. 17. Model for buzz noise mitigation. (a) Case 1: adding the decoupling capacitor at the internal node. (b) Case 2: adding the decoupling capacitor at the input of Mic codec IC.

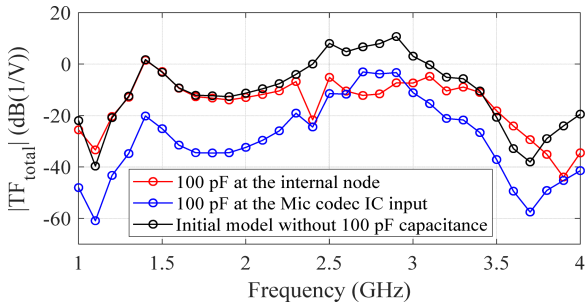

Fig. 18. Comparison of the TF_{total} between adding the decoupling capacitor at the input of Mic codec IC, adding the decoupling capacitor at the internal node and the original model.

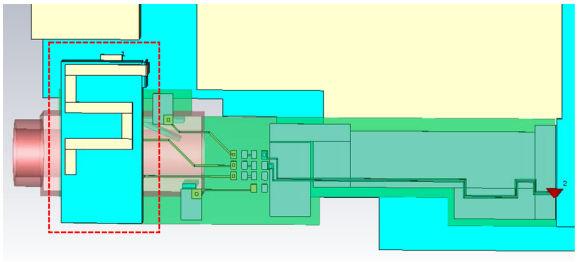

Fig. 19. 3-D model with the new antenna structure.

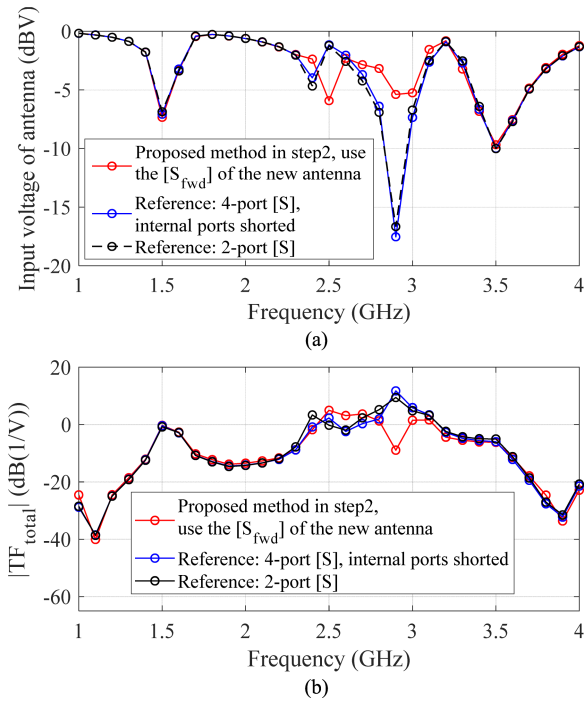

Fig. 20. Comparison between the terms simulated from the two-port S-parameter, four-port S-parameter, and the proposed circuit model with only the $[S_{\mathrm{fwd}}]$ replaced with the new antenna model. (a) U_{antenna}. (b) $\mathrm{TF}_{\mathrm{total}}$.

B. Buzz Noise Prediction With Different Antenna Structures

The proposed model can also estimate the buzz noise for different antenna structures and achieve fast antenna selection with lower accuracy. Fig. 19 shows the 3-D simulation models with the new antenna structure. When using the same Huygens box and cell dimensions, the U_{antenna} and $\mathrm{TF}_{\mathrm{total}}$ simulated in the proposed SPICE-compatible model are compared with the results simulated from the two-port and four-port S-parameter matrices directly from CST, as shown in Fig. 20. For the new antenna structure in the proposed model, only $[S_{\mathrm{fwd}}]$ is regenerated with the fields in the forward problem from the new antenna model. $[S_{\mathrm{rev}}]$ remains the same as that from the original antenna structure model to reduce the simulation time.

As shown in Fig. 20, when replacing $[S_{\mathrm{fwd}}]$ with the new antenna structure, the proposed model can still predict the $\mathrm{TF}_{\mathrm{total}}$ within an acceptable accuracy (average error of 2.2 dB). The discrepancies of $\mathrm{TF}_{\mathrm{total}}$ are caused by larger discrepancies in the simulated U_{antenna}, which are from the errors induced by using $[S_{\mathrm{rev}}]$ extracted from the model with the original antenna structure. $[S_{\mathrm{rev}}]$ in the model with new antenna structure will be affected by the scattering effect of the new antenna structure. Overall, the proposed model shows the feasibility of fast predicting the buzz noise with different antenna structures by updating $[S_{\mathrm{fwd}}]$ only and sacrificing the accuracy on the scattering effect between the new antenna and victim structure.

C. Discussion

The advantage of the proposed model is that it provides a fast method during the predesign stage of a product on buzz noise prediction, coupling decomposition from aggressor to different parts of the victim, buzz noise mitigation, and antenna selection.

The disadvantage of the proposed model is that the accuracy is limited by the cell size of the discretized surfaces on the Huygens box. Besides, the simulation time will increase significantly if a large number of cells are used. Therefore, a suitable Huygens box and cell size are needed, which is a tradeoff between the simulation time and accuracy.

V. Conclusion

In this article, a SPICE-compatible model is proposed to characterize the buzz noise problem in a camera device. It consists of cascaded S-parameter matrices generated from the field coupling based on the reciprocity theorem. The proposed SPICE-compatible model allows for a fast (≦6.1 min) and accurate (average error of 1 dB) estimation of the total transfer function between the RF antenna and the induced buzz noise and coupling decomposition. Instead of performing multiple times 3-D full-wave simulation, the proposed model can provide fast buzz noise mitigation with only one-time 3-D simulation, and antenna structure selection with reduced-time 3-D simulation. The limitation of the proposed model lies in that the accuracy and simulation time is a tradeoff due to the discretization of the Huygens box in the reciprocity theorem.

Appendix A
TFIC Measurement and Definition Under Square-Law Demodulation Hypothesis

The method to extract the TF_{IC} in (4) is from measurement method described in [6]. First, the WiFi antenna was disabled and the connection of the audio path to the input pin of the Mic codec IC is disconnected. This was to make sure no WiFi-antenna-coupled noise at the input of Mic codec IC and the Mic codec IC was working as a "standalone" status without any audio signal or noise from the camera system. Then a three-tone mixed signal ($f_{\mathrm{IF}} = 1$ kHz, sweep the f_{LO} from 1 to 4 GHz) was created through a mixer as the RF signal with modulation. The three-tone signal was intentionally injected into the audio input pin of the Mic codec IC through a short semirigid coaxial cable. Meanwhile, the camera was powered on and recording the audio data from the Mic codec IC. Finally, by analyzing the spectrum of the recorded audio data, we were able to get the baseband frequency components at 1 kHz (f_{IF}) and 2 kHz ($2f_{\mathrm{IF}}$).

As was discussed in [6], the square operation on the modulated signal with low-pass filter and certain scaling coefficient can reproduce the demodulation behavior of the nonlinear device in the audio circuit. Suppose a three-tone signal $y_0(t)$ with intermediate frequency of f_{IF} (in kilohertz range below 20 kHz) and local oscillator frequency f_{LO} (in gigahertz range) generated by the mixer, which is expressed as follows:

$$\begin{aligned} &y_0(t) \\ &\quad = U_{f_{LO}} \sin(2\pi f_{LO} t) + U_{f_{LO}+f_{IF}} \sin(2\pi(f_{LO}+f_{IF})t) \\ &\quad + U_{f_{LO}-f_{IF}} \sin(2\pi(f_{LO}-f_{IF})t) \end{aligned} \tag{14}$$

Where $U_{f_{LO}}$, $U_{f_{LO}+f_{IF}}$, and $U_{f_{LO}-f_{IF}}$ are the amplitudes of the mixed signal at frequencies of f_{LO}, $f_{\mathrm{LO}}+f_{\mathrm{IF}}$, and $f_{\mathrm{LO}}-f_{\mathrm{IF}}$, respectively.

Next, suppose the nonlinear effect of the Mic codec IC is a square operation on $y_0(t)$ and after a low-pass filter effect with certain scaling coefficient in the magnitude, the audio signal ($<$ 20 kHz) with buzz noise can be reproduced. From (15) shown at the bottom of this page, the spectrum of $y_0(t)^2$ contains dc component, RF components at frequencies of $2f_{LO}$, $2f_{\mathrm{LO}}+f_{\mathrm{IF}}$, and $2f_{\mathrm{LO}}-f_{\mathrm{IF}}$, base-band frequency components at f_{IF} and 2 f_{IF} representing the buzz noise components. Therefore, by applying a square operation and a low-pass filter ($<$ 20 kHz) with certain coefficient (A_c) to the input RF signal with modulation, we can extract the total buzz noise in the audio signal, as shown in (16)

$$\begin{aligned} &\text{Total buzz noise} \\ &= A_c \begin{bmatrix} (U_{f_{LO}} U_{f_{LO}+f_{IF}} + U_{f_{LO}} U_{f_{LO}-f_{IF}}) \cos(2\pi(f_{IF})t) \\ -U_{f_{LO}+f_{IF}} U_{f_{LO}-f_{IF}} \cos(2\pi(2f_{IF})t) \end{bmatrix}. \end{aligned} \tag{16}$$

The magnitude of the $2f_{\mathrm{IF}}$ component in the total buzz noise is only related to the magnitude of the modulated RF signal components of $y_0(t)$. The magnitude of f_{IF} component in the buzz noise is related to the magnitude of the input signal at f_{LO} and at $f_{\mathrm{LO}}\pm f_{\mathrm{IF}}$ (modulated RF signals). Since the WiFi signal is always a modulated RF signal, a better quantification of the buzz noise in the three-tone-signal-injection measurement should be using the magnitude of the component at $2f_{\mathrm{IF}}$ (2 kHz in this example). Besides, assuming the difference of the amplitude of $y_0(t)$ at $f_{LO}+f_{IF}$ and $f_{LO}-f_{IF}$ is negligible ($U_{f_{LO}\pm f_{IF}} = U_{f_{LO}+f_{IF}} = U_{f_{LO}-f_{IF}}$), the amplitude of component at $2f_{\mathrm{IF}}$ is proportional to $U^2_{f_{LO}\pm f_{IF}}$. Therefore, by obtaining $\sqrt{\mathrm{Buzz}}$ at $2f_{\mathrm{IF}}$ and dividing the $\sqrt{\mathrm{Buzz}}$ by the amplitude of $y_0(t)$ at $f_{\mathrm{LO}}+f_{\mathrm{IF}}$, the transfer function TF_{IC} can represent the scaling factor $\sqrt{A_0}$ between the amplitude of $\sqrt{\mathrm{Buzz}}$ at $2f_{\mathrm{IF}}$ and the voltage amplitude of the applied modulated RF signal at $f_{\mathrm{LO}}\pm f_{\mathrm{IF}}$ at the input of the Mic codec IC (considering Z_{IC}, the input impedance of the audio input pin of the Mic codec IC).

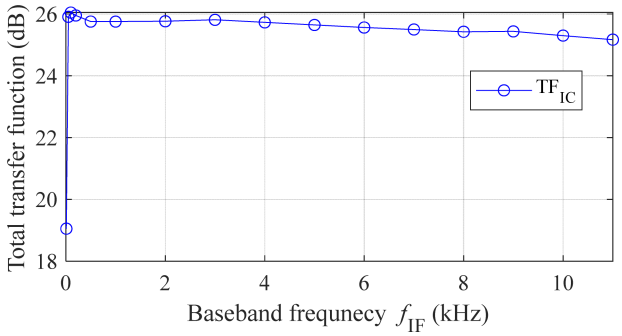

Fig. 21. TF_{IC} versus baseband frequency (f_{IF}) under carrier frequency of 2.4 GHz.

The measured TF_{IC} versus baseband frequency in the modulated signal (carrier frequency = 2.4 GHz) is shown in Fig. 21, indicating a constant response of TF_{IC} with the baseband frequency in 50–11 kHz.

Appendix B
Detailed SPICE Simulation Model

The SPICE simulation in this article was performed in Agilent Advanced Design System 2017 (ADS 2017) [25]. Taking an example of Fig. 14 in this article, the detailed simulation model is shown in Fig. 22 for further explanation. Fig. 22(a) shows the whole model structure containing the antenna excitation, cascade S-parameters of field coupling, termination of Z_{IC}, calculation of U_{IC} and $\sqrt{Buzz}$. Fig. 22(b)–(d) shows the detailed circuit model built in ADS for simulation to obtain U_{antenna}, U_{IC}, and $\sqrt{Buzz}$, from which the $\mathrm{TF}_{\mathrm{total}}$ can be obtained by $\sqrt{\mathrm{Buzz}}/U_{\mathrm{antenna}}$. Fig. 22(b) shows the block for generating the excitation of the antenna (U_{antenna}). Fig. 22(c) shows the zoom-in picture for the model connection in the top surface (x–y plane) of the Huygens box, which is the same connection structure, as shown in Fig. 9 in this article. The forward E and H fields in x and y directions in the 299 discretized cells of the top surface were expressed with four S-parameter files ($[S_{\mathrm{fwd}}]$). The reverse E and H field in x and y directions in the discretized cells of the top surface were expressed with four S-parameter files ($[S^1_{rev}]$) when exciting the Mic jack port (Port 3 in Fig. 5) in Mic jack region with other ports terminated with 50 Ω and another four S-parameter files of $[S^2_{rev}]$ when exciting the victim port (Port

$$\begin{aligned} y_0(t)^2 &= (U_{f_{LO}} \sin(2\pi f_{LO} t) + U_{f_{LO}+f_{IF}} \sin(2\pi(f_{LO}+f_{IF})t) + U_{f_{LO}-f_{IF}} \sin(2\pi(f_{LO}-f_{IF})t))^2 \\ &= \tfrac{1}{2}\left({U_{f_{LO}}}^2 + {U_{f_{LO}+f_{IF}}}^2 + {U_{f_{LO}-f_{IF}}}^2\right) + \left(U_{f_{LO}+f_{IF}} U_{f_{LO}-f_{IF}} - {U_{f_{LO}}}^2/2\right)\cos(2\pi 2 f_{LO} t) \\ &\quad + \left(U_{f_{LO}} U_{f_{LO}+f_{IF}} - {U_{f_{LO}+f_{IF}}}^2/2\right)\cos(2\pi(2f_{LO}+f_{IF})t) \\ &\quad + \left(U_{f_{LO}} U_{f_{LO}-f_{IF}} - {U_{f_{LO}-f_{IF}}}^2/2\right)\cos(2\pi(2f_{LO}-f_{IF})t) \\ &\quad - (U_{f_{LO}} U_{f_{LO}+f_{IF}} + U_{f_{LO}} U_{LO-f_{IF}})\cos(2\pi(f_{IF})t) - U_{f_{LO}+1kHz} U_{LO-1kHz}\cos(2\pi(2f_{IF})t) \end{aligned} \tag{15}$$

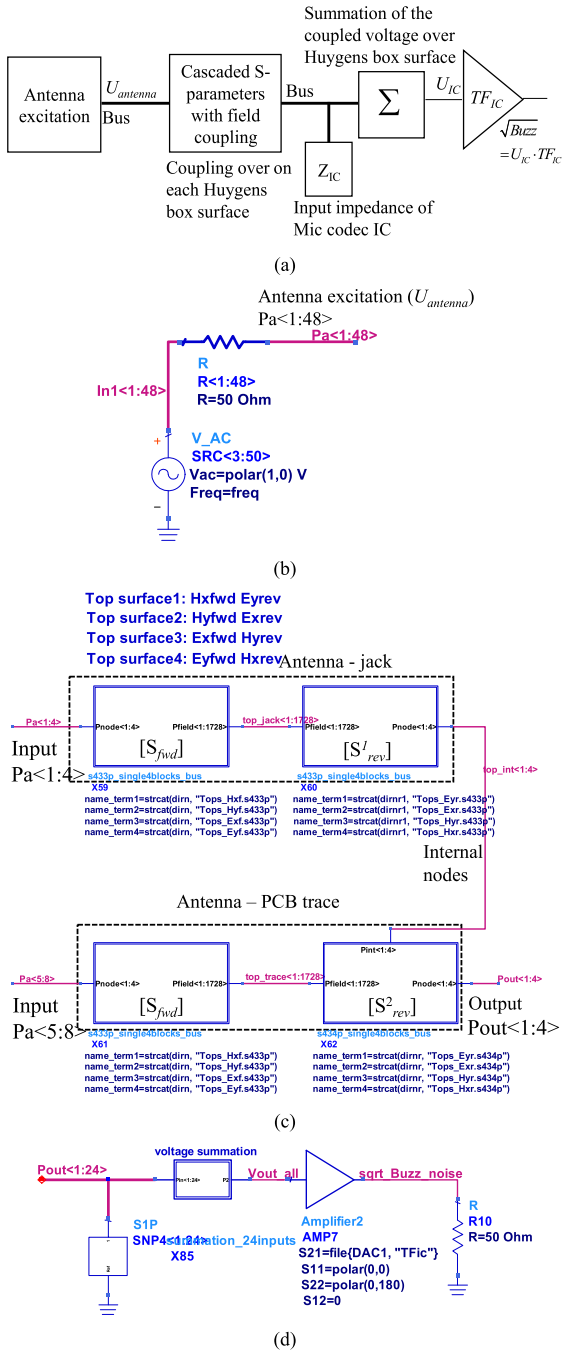

Fig. 22. Detailed circuit model in ADS for transfer function (TF_{total}) simulation. (a) Connection diagram. (b) Excitation source for antenna. (c) Cascaded S parameter matrix with field coupling for coupling between antenna and top surface of Huygens box. (d) Termination of Mic codec IC, summation of the coupled voltage from six surfaces of Huygens box, and $\sqrt{Buzz}$ simulation with TF_{IC}.

2 in Fig. 5) in PCB trace region with other ports terminated with 50 Ω. By cascading the $[S_{fwd}]$with $[S^{1}_{rev}]$and $[S^{2}_{rev}]$, the product of the forward and reverse field terms in the same cell can be achieved. Similar models were built for bottom, left, right, front, and back surfaces of the Huygens box to obtain the coupling between the antenna and victim through each surface of the Huygens box. Fig. 22(d) shows the connection for the input impedance of the Mic codec IC audio pin (left channel) and the summation of all the coupled voltage at the input of the Mic codec IC, which is contributed from the field couplings in the six surfaces of the Huygens box. Therefore, U_{IC} is obtained. Finally, by applying the coefficient of TF_{IC}, the $\sqrt{\text{Buzz}}$ can be simulated and the TF_{total} can be extracted, as is shown in Figs. 15 and 16.

REFERENCES

[1] M. Skopec, "Hearing aid electromagnetic interference from digital cellular telephones," in *Proc. 18th Annu. Int. Conf. IEEE Eng. Med. Biol. Soc.*, Amsterdam, The Netherlands, 1996, pp. 409–410.

[2] M. Skopec, "Hearing aid electromagnetic interference from digital wireless telephones," *IEEE Trans. Rehabil. Eng.*, vol. 6, no. 2, pp. 235–239, Jun. 1998.

[3] T. Instruments, "AN-1496 noise, TDMA noise, and suppression techniques," Texas Instrum., Dallas, TX, USA, Rep. SNAA033D, May 2006. [Online]. Available: https://www.ti.com/lit/an/snaa033d/snaa033d.pdf?ts=1611699217422&ref_url=https%253A%252F%252Fwww.google.com%252F

[4] B. Poole, "Reducing audio 'buzz' in GSM cell phones," *EDN*, pp. 67–70, Feb. 2005.

[5] R. E. Schlegel and F. H. Grant, "Modeling the electromagnetic response of hearing aids to digital wireless phones," *IEEE Trans. Electromagn. Compat.*, vol. 42, no. 4, pp. 347–357, Nov. 2000.

[6] Y. Zhong, Q. Huang, T. Enomoto, S. Seto, K. Araki, and C. Hwang, "Measurement-based characterization of buzz noise in wireless devices," in *Proc. IEEE Symp. Electromagn. Compat., Signal Integrity Power Integrity*, Long Beach, CA, USA, 2018, pp. 134–138.

[7] Y. Zhong *et al.*, "Measurement-based quantification of buzz noise in wireless devices," in *Proc. Joint Int. Symp. EMC Sapporo/APEMC*, Sapporo, Japan, 2019, pp. 552–555.

[8] V. Barbaro *et al.*, "On the mechanisms of interference between mobile phones and pacemakers: Parasitic demodulation of GSM signal by the sensing amplifier," *Phys. Med. Biol.*, vol. 48, no. 11, pp. 1661–1671, Jun. 2003.

[9] S. Park, S. Jinwook, K. Subin, L. Manho, K. Jonghoon, and K. Joungho, "Audio frequency ground integrity modeling and measurement for a TDMA smartphone system," in *Proc. IEEE Elect. Des. Adv. Packag. Syst.*, Honolulu, HI, USA, 2016, pp. 3–5.

[10] S. Park, J. Song, S. Kim, Y. Kim, M. Lee, and J. Kim, "Modeling, measurement, and analysis of audio frequency ground integrity for a TDMA smartphone system," *IEEE Trans. Compon. Packag. Manuf. Technol.*, vol. 8, no. 4, pp. 519–530, Apr. 2018.

[11] H. Wang, V. Khilkevich, Y. Zhang, and J. Fan, "Estimating radio-frequency interference to an antenna due to near-field coupling using decomposition method based on reciprocity," *IEEE Trans. Electromagn. Compat.*, vol. 55, no. 6, pp. 1125–1131, Dec. 2013.

[12] L. Li *et al.*, "Measurement validation for radio-frequency interference estimation by reciprocity theorem," in *Proc. IEEE Int. Symp. Electromagn. Compat.*, Dresden, Germany, 2015, pp. 154–159.

[13] J. Pan *et al.*, "Radio-frequency interference estimation using equivalent dipole-moment models and decomposition method based on reciprocity," *IEEE Trans. Electromagn. Compat.*, vol. 58, no. 1, pp. 75–84, Feb. 2016.

[14] L. Li *et al.*, "Near-field coupling estimation by source reconstruction and Huygens's equivalence principle," in *Proc. IEEE Symp. Electromagn. Compat. Signal Integrity*, Santa Clara, CA, USA, 2015, pp. 324–329.

[15] Q. Huang *et al.*, "Reciprocity theorem based RFI estimation for heatsink emission," in *Proc. IEEE Int. Symp. EMC+SIPI*, New Orleans, LA, USA, 2019, pp. 590–594.

[16] Q. Huang, Y. Liu, L. Li, Y. Wang, C. Wu, and J. Fan, "Radio frequency interference estimation using transfer function based dipole moment model," in *Proc. IEEE Int. Symp. Electromagn. Compat. IEEE Asia-Pacific Symp. Electromagn. Compat.*, Suntec City, Singapore, 2018, pp. 115–120.

[17] Q. Huang, T. Enomoto, S. Seto, K. Araki, J. Fan, and C. Hwang, "Accurate and fast RFI prediction based on dipole moment sources and reciprocity," in *Proc. DesignCon*, 2018.

[18] Q. Huang *et al.*, "A novel RFI mitigation method using source rotation," *IEEE Trans. Electromagn. Compat.*, vol. 63, no. 1, pp. 11–18, Feb. 2021.

[19] G. Johnson, "Oriented PIFA-type device and method of use for reducing RF interference," U.S. Patent 7 230 574, Jun. 12, 2007.

[20] T. E. Miller and A. D. Unruh, "Prevention of buzz noise in smart microphones," U.S. Patent 16 846 123, Oct. 15, 2020.
[21] I. Claesson and A. Rossholm, "Notch filtering of humming GSM mobile telephone noise," in *Proc. 5th Int. Conf. Inf. Commun. Signal Process.*, Bangkok, Thailand, 2005, pp. 1320–1323.
[22] T. Kim and S. Kim, "A method for reducing a bumblebee noise generated by a GSM technology in a smartphone," in *Proc. 12th Int. Conf. Intell. Syst. Des. Appl*, Kochi, IL, USA, 2012, pp. 927–930.
[23] R. G. Garratt and E. V. Carlson, "System for mitigating RF interference in a hearing aid," U.S. Patent 6 307 944, Oct. 23, 2001.
[24] CST MICROWAVE STUDIO, CST Computer Simulation Technology, 2017. [Online]. Available: https://www.cst.com/2017
[25] Advanced Design System, Keysight Technologies, 2017. [Online]. Available:https://www.keysight.com/us/en/lib/resources/software-releases/ads-2017.html

Wei Zhang (Student Member, IEEE) received the B.S. degree in electronic information engineering from Central South University, Changsha, China, in 2014, and the M.S. degree in electronic science and technology from Beihang University, Beijing, China, in 2017. She is currently working toward the Ph.D. degree in electrical engineering with Electromagnetic Compatibility Laboratory, Missouri University of Science and Technology, Rolla, MO, USA.

Her current research interests include measurement and analysis in system EMI and RFI.

Shengxuan Xia (Graduate Student Member, IEEE) received the B.S. degree in electrical and computer engineering from the Huazhong University of Science and Technology, Wuhan, China, in 2018. He is currently working toward the Ph.D. degree in electrical engineering with the Electromagnetic Compatibility Laboratory, Missouri University of Science and Technology, Rolla, MO, USA.

His research interests include radio-frequency interference, desense, radiated emission susceptibility modeling, and hardware security.

Xin Fang (Graduate Student Member, IEEE) received the B.E. degree in electronic science and technology from Zhejiang University, Hangzhou, China, in 2019. She is currently working toward the M.S. degree in electrical engineering with Electromagnetic Compatibility Laboratory, Missouri University of Science and Technology, Rolla, MO, USA.

Her research interests include making IC model for EMI problems prediction, RFI analysis for camera model, and PDN modelling for ultralow impedance PCBs.

Xu Wang (Graduate Student Member, IEEE) received the B.S. and M.S. degrees in electrical engineering from the University of Electronic Science and Technology of China, Chengdu, China, in 2015 and 2018, respectively. He is currently working toward the Ph.D. degree in electrical engineering with the Missouri University of Science and Technology, Rolla, MO, USA.

His current research interests include partial element equivalent circuit modeling and development of radiation emission models for components and devices

Takashi Enomoto received the B.S. degree in electrical engineering from the Kyoto Institute of Technology, Kyoto, Japan, in 1989.

He joined Sony Corporation as an Electrical Engineer in 1989. His research interests include development of ESD/RFI measurement and simulation techniques.

Hideki Shumiya received the B.S. and M. S. degrees in electrical engineering from Nagoya University, Nagoya, Japan, in 2003 and 2006, respectively.

After working with Tokai-Rika Corporation as an Electrical Designer of automotive products for one year, he joined Sony Corporation as an Electrical Engineer in 2007. His research interests include development of EMC design guideline, ESD measurement, and simulation techniques.

Kenji Araki (Senior Member, IEEE) received the B.S. and M.S. degrees in electrical engineering from Hosei University, Koganei, Japan, in 1991 and 1993, respectively, and the Ph.D. degree in electrical engineering from The University of Electro-Communications, Chofu, Japan, in 2009.

He joined Sony Corporation as an Electrical Engineer in 1993, and is currently a General Manager of Sony Global Manufacturing & Operations Corporation, Tokyo, Japan. His research interests include signal integrity, power integrity, electromagnetic interference, electrostatic discharge, radio frequency interference, and simulation for electromagnetic compatibility.

Dr. Araki is a Senior Member of the Institute of Electronics, Information and Communication Engineers of Japan. He was the recipient of an IEEE EMC Society Technical Achievement Award in May 2018.

Chulsoon Hwang (Senior Member, IEEE) received the B.S., M.S., and Ph.D. degrees in electrical engineering from the Korea Advanced Institute of Science and Technology, Daejeon, South Korea, in 2007, 2009, and 2012, respectively.

From 2012 to 2015, he was with Samsung Electronics, Suwon, South Korea, as a Senior Engineer. In July 2015, he joined the Missouri University of Science and Technology (formerly University of Missouri-Rolla), Rolla, MO, USA, where he is currently an Assistant Professor. His research interests include RF desense, signal/power integrity in high-speed digital systems, EMI/EMC, hardware security, and machine learning.

Dr. Hwang was a recipient of the AP-EMC Young Scientist Award, the Google Faculty Research Award, and Missouri S&T's Faculty Research Award. He was a corecipient of the IEEE EMC Best Paper Award, the AP-EMC Best Paper Award, and a two-time corecipient of the DesignCon Best Paper Award.